Shape-transformation of polymersomes from glassy and crosslinkable ABA triblock copolymers

Tamuka Chidanguro, Elina Ghimire, and Yoan C. Simon*

School of Polymer Science and Engineering, The University of Southern Mississippi,

118 College Dr. #5050 Hattiesburg 39406 MS USA

E-mail:yoan.simon@usm.edu

Abstract

Recent developments in the field of polymer vesicles, i.e. *polymersomes*, have demonstrated that disrupting the equilibrium conditions of the milieu could lead to shape transformation into stable non-spherical morphologies, bringing on-demand shape control to reality and bearing great promise for cell mimicry and a variety of biomedical applications. Here, we studied the self-assembly behavior of glassy amphiphilic triblock copolymers, poly(ethylene glycol)-*block*-polystyrene-*stat*-poly(coumarin methacrylate)-*block*-poly(ethylene glycol) (PEG-*b*-P(S-*stat*-CMA)-*b*-PEG), and their response to various stimuli. By changing the respective molecular weights of both the hydrophobic P(S-*stat*-CMA) and the hydrophilic PEG blocks, we varied the hydrophobic volume fraction thereby accessing a range of morphologies from spherical and worm-like micelles, as well as polymersomes. For the latter, we observed that slow osmotic pressure changes induced by dialysis led to a decrease in size while rapid osmotic pressure changes by addition of a PEG fusogen led to morphological transformations into rod-like and tubular polymersomes. We also found out that chemically crosslinking the vesicles before inducing osmotic pressure changes led to the vesicles exhibiting hypotonic shock, atypical for glassy polymersomes. We believe that this approach combining the robustness of triblock copolymers

and light-based transformations will help expand the toolbox to design ever more complex biomimetic constructs.

1. Introduction

Since the late 1990s, the self-assembly of amphiphilic block copolymers has expanded the toolkit to design complex biomimetic architectures at the nanoscale from the bottom up.[1,2] Polymersomes (also known as polymer vesicles) have especially garnered much interest because of their unique cell-like structure, whereby amphiphilic macromolecules form a membrane separating the inside (or lumen) of the polymersome from its outside. As a result, they can encapsulate both hydrophilic cargo in their lumen and/or carry hydrophobic molecules within their membrane.[3] Their tunable permeability can even allow them to function as nanoreactors,[4] akin to organelles in the body. For instance, trypsin displayed increased activity towards a BZiPAR (Rhodamine 110, bis-(*N*-CBZ-L-isoleucyl-L-prolyl-L-arginine amide), dihydrochloride) substrate when encapsulated in poly(2-methyloxazoline)-*block*-poly(dimethylsiloxane)-*block*-poly(2-methyloxazoline) vesicles.[5,6] As a result, polymer vesicles are highly desirable in diverse areas of research ranging from catalysis,[7] cellular modelling,[8,9] drug delivery,[10] to bioimaging and diagnostics.[11,12]

Since polymersomes are becoming increasingly useful, their shape control is now proving to be the next frontier. Cellular organelles, bacteria, and viral capsids exist in a plethora of morphologies that allow them to efficiently carry out their functions. As we aspire to replicate these complex, compartmentalized, biological architectures, it becomes essential to diverge from simple spherical morphologies to access a broad array of shapes and structures that will enable new functionalities.[13,14] In drug delivery, tubular and rod-like structures offer higher loading efficiencies compared to their spherical analogs. Additionally, their large surface area enhances

cellular uptake,[15-17] and, in the bloodstream, particle geometry affects the hemodynamic (drag) and buoyancy forces which govern the particle trajectory.[18-20]

Various groups have recently explored the ability of polymersomes to achieve non-spherical morphologies, such as stomatocytes, tubular and nested polymersomes.[17,21,22] For instance, the groups of van Hest and Wilson demonstrated that the addition of water-miscible organic solvents plasticized the membrane of polymersomes made from block copolymers containing glassy hydrophobic segments, such as polystyrene-*block*-poly(ethylene glycol) (PS-*b*-PEG) and poly(D,L-lactide)-*block*-poly(ethylene glycol) (PDLLA-*b*-PEG), and enabled their shape manipulation.[21] They could *kinetically freeze* or *quench* these non-spherical morphologies by adding them into water thereby vitrifying the PS and PDLLA blocks and exploited these structures in applications, such as drug delivery or nanomotors.[23]

Due to their very nature, ABA triblock copolymers possess the ability to span the vesicular membrane bridging the inside and outside of the polymersome.[24,25] This unique characteristic significantly enhances their stability and ability to withstand changes in osmotic pressure. For copolymers consisting of a hydrophilic PEG block and a soft hydrophobic poly(dimethylsiloxane) block, Salva et al compared the responses of polymersomes made from diblock and triblock copolymers to hypertonic salt solutions by cryogenically freezing the otherwise unstable intermediates.[26] They found that the diblock-based polymersomes transformed beyond stomatocytes into nested polymersomes upon fusion of the membrane. Comparatively, while they could manipulate triblock-based vesicles to form stomatocytes, the ABA architecture precluded membrane fusion and the formation of nested structures.

To the best of our knowledge, and despite the advantageous mechanical properties of triblock copolymers, all of the reports to date on the shape-transformation of glassy polymersomes

have focused on diblock copolymers. We have therefore designed an amphiphilic triblock copolymer poly(ethylene glycol)-*block*-poly(styrene-*stat*-(coumarin methacrylate))-*block*-poly(ethylene glycol) (PEG-*b*-P(S-*stat*-CMA)-*b*-PEG). We hypothesized that slow and rapid osmotic pressure changes, respectively via dialysis and the use of a PEG fusogen, would lead to an area-mismatch between the vesicle membrane interior and exterior, and to shape transformation. We originally posited that UV-induced [2+2] cycloaddition dimerization of the coumarin moiety would enable easy crosslinking of the polymersomes, lower their permeability to water and thereby facilitate their shape transformation. As demonstrated in the following paragraphs, this assumption turned out to be erroneous and crosslinking resulted in a presumed increase in permeability. Most importantly, we expected that the glassy nature of the vesicle hydrophobic membrane would allow us to isolate stable non-spherical polymersomes. Interestingly, osmotic pressure changes via dialysis and rapid changes using a PEG fusogen led to markedly different responses for the vesicles, demonstrating the delicate nature of these out-of-equilibrium shape-changes.

2. Results and Discussion

2.1 Synthesis of amphiphilic block copolymers

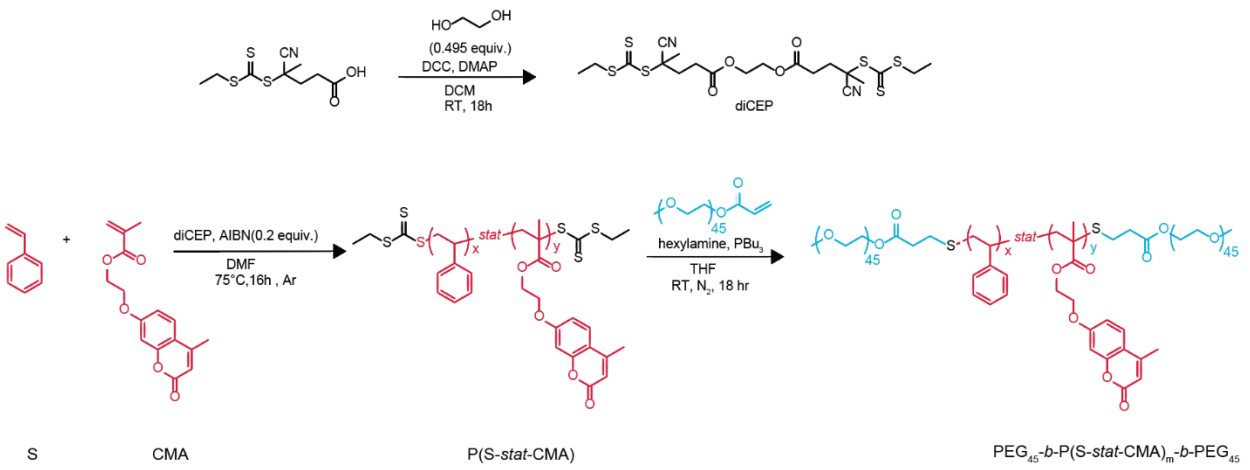

Scheme 1. (Top) Synthesis of the difunctional chain-transfer agent (diCEP) via Steglich esterification. (Bottom) Synthesis of amphiphilic triblock copolymers via RAFT copolymerization of styrene (S) and coumarin methacrylate (CMA) followed by one-pot aminolysis and thia-Michael addition of methoxy poly(ethylene glycol) acrylate (mPEGA). Note that, for the simplicity of the representation of the copolymers, the central diCEP subunit is omitted. As a result, the bonds connecting the trithiocarbonate and thioether moieties to the P(S-*stat*-CMA) block on the left-hand side are not representative of the actual regiochemistry and therefore simply depicted as a purple line.

To synthesize the amphiphilic triblock copolymers, we designed a difunctional chain-transfer agent (CTA), whose structure allows divergent reversible addition-fragmentation chain-transfer (RAFT). This approach enables the easy post-polymerization functionalization of the thiocarbonylthio end groups flanking the telechelic hydrophobic core.[27,28] To this end, we first synthesized cyano-4-(ethylsulfanylthiocarbonylsulfanyl)pentanoic acid (CEP) using a known procedure,[29] followed by a Steglich esterification with ethylene glycol (Scheme 1) to yield the subsequent difunctional CTA (diCEP). The shift of the ethylene glycol methylene proton peaks at

3.76 ppm to 4.33 ppm and the disappearance of the OH peak at 3.17 ppm confirmed the success of the esterification reaction (Figure S2-3).

While S and CMA have been copolymerized before,[30] we wanted to establish whether the coumarin moiety would be randomly distributed throughout the membrane. We carried out the diCEP-mediated RAFT copolymerization in DMF at 75 °C with a 1:4 molar ratio of CMA:S and took out aliquots at five time points between 4 and 20 hours (Scheme S1). After precipitating the aliquots in methanol and drying them overnight under vacuum, we then used ^{1}H NMR spectroscopy to compare the ratio of the alkene proton at 6.13 ppm characteristic of the coumarin to the aromatic region between 6.33 ppm and 7.55 ppm comprising the aromatic signals of both styrene and coumarin (Figure S4). For all time-points, we observed a ratio of 14.1-17.8 between the alkene and aromatic regions, indicating that the final polymers had a final CMA:S ratio between 1:2.23 and 1:2.95 (Table S1). These results suggest that the polymers contained a slightly higher CMA content compared to the initial monomer mixture. However, the fluctuation in this ratio throughout the polymerization suggested that the monomer addition largely followed a random incorporation.

We then synthesized seven hydrophobic blocks with molecular weights ranging from 8 500 g/mol to 32 000 g/mol targeting 50% monomer conversion (Table 1) and using a 1:4 molar ratio of CMA:S. We used a low diCEP:initiator ratio of 1:0.2 (1:0.1 ratio for each CTA functionality) to ensure that the polymers would have more than 90% living chains.[31] We found that the CMA:S ratio was comprised between 1:2.03 and 1:3.0 (Figure S5 and Table S2). The use of acetone-d_6 ensured that the solvent peaks would not coincide with polymer signals. Overall, the target and experimentally measured molecular weights by size-exclusion chromatography (SEC) agreed (Table 1 and Figure S6, black SEC traces). Satisfyingly, all chromatograms showed a narrow

monomodal molecular weight distribution with $Đ$ = 1.11 – 1.23. We then performed a one-pot aminolysis of the trithiocarbonate end groups and thia-Michael coupling reaction with methoxy poly(ethylene glycol) acrylate (mPEGA) to yield the ABA triblock copolymers. While soft amphiphilic block copolymers typically self-assemble into vesicular morphologies at $0.25 \leq f \leq 0.45$, where f is defined as the hydrophilic fraction, glassy diblock copolymers often require a much lower f.[32] We therefore utilized two PEG acrylate blocks with molecular weights of 1 000 g/mol (PEG_{22}) and 2 000 g/mol (PEG_{45}) to synthesize seven triblock copolymers in order to access vesicle morphologies. Conveniently, the disappearance of the characteristic yellow color of the CTA during the reaction was a good visual indicator of the successful aminolysis. The shift towards lower retention times (Figure S6, red SEC traces) further confirmed the efficiency of the thia-Michael addition. Fortunately, the shape of the SEC traces also remained unchanged (except for PEG_{22}-*b*-P(S-*stat*-CMA)$_{136}$-*b*-PEG_{22} where a small low-molecular weight shoulder appeared), confirming the completion of the reaction. This clean shift is particularly apparent for PEG_{45}-*b*-(S-*stat*-CMA)$_{70}$-*b*-PEG_{45} (Figure S6d) and overall, the dispersity remained low ($Đ$ = 1.09 – 1.20). Nevertheless, due to inconsistencies in the refractive index increment values obtained by SEC assuming 100% mass recovery (Table S4), we relied on ^{1}H NMR spectroscopic data to accurately evaluate the molecular weight of the triblocks.

The appearance of the characteristic PEG peak at 3.64 ppm and the absence of any signal between 5.65 and 5.95 ppm further corroborated the achievement of the thia-Michael addition (Figure S7). Based on the P(S-*stat*-CMA) molecular weight obtained by SEC and the CMA content previously determined by ^{1}H NMR spectroscopy, we used the integration ratio of the PEG protons to the characteristic coumarin alkene protons to determine the M_n of the corresponding PEG-*b*-P(S-*stat*-CMA)-*b*-PEG triblocks (Tables 1 and S3, Figure S8 and subsequent explanation in ESI).

For the PEG_{22} series, the experimental M_n line up remarkably well with the values expected at full completion of the thia-Michael coupling reaction. We note however that the experimental M_n values appear to be ever so slightly below for the larger PEG_{45} which could potentially stem from a less quantitative though efficient coupling for the larger PEG blocks. The integration ratios of the PEG protons to the alkene protons also enabled the determination of f for each triblock, with $0.08 \leq f \leq 0.24$.

Table 1. Characterization of the triblock copolymers synthesized and their intermediates and the hydrophilic volume fractions

	P(S-*stat*-CMA)				Triblock		
Polymer Identity[a]	$M_{n\ theo}$ [b] **(g/mol)**	$M_{n\ exp}$ [c] **(g/mol)**	**CMA content[d]**	$Đ$ [c]	M_n [e] **(g/mol)**	$Đ$ [c]	f [e] **(%)**
PEG_{22}-*b*-P(S-*stat*-CMA)$_{56}$-*b*-PEG_{22}	6 000	8 500	0.26	1.11	10 500	1.10	19
PEG_{22}-*b*-P(S-*stat*-CMA)$_{104}$-*b*-PEG_{22}	16 000	15 500	0.25	1.12	17 500	1.11	12
PEG_{22}-*b*-(S-*stat*-CMA)$_{118}$-*b*-PEG_{22}	17 500	18 000	0.27	1.11	20 300	1.09	11
PEG_{22}-*b*-P(S-*stat*-CMA)$_{136}$-*b*-PEG_{22}	20 000	20 900	0.27	1.13	22 800	1.17	8
PEG_{45}-*b*-(S-*stat*-CMA)$_{70}$-*b*-PEG_{45}	10 000	10 500	0.25	1.11	13 800	1.13	24

PEG_{45}-*b*-(S-*stat*-CMA)$_{170}$-*b*-PEG_{45}	30 000	27 800	0.32	1.17	31 300	1.18	13
PEG_{45}-*b*-(S-*stat*-CMA)$_{206}$-*b*-PEG_{45}	43 000	32 000	0.28	1.23	35 700	1.20	10

[a]The number-average degree of polymerization (DP_n) of the central of block is the average number of structural units per polymer chain. The molecular weight of the statistical repeat unit was calculated based on the molecular weights and ratio of S:CMA in the final polymer as determined by ^{1}H NMR. [b]Targeted molecular weight based on 50% monomer conversion. [c]As determined by SEC (THF). [d]Calculated based on aromatic/alkene ratio in the polymer ^{1}H NMR (see Figure S5 and Table S2). [e]Determined via ^{1}H NMR (see Figure S8 and Table S3).

2.2 Self-assembly of the amphiphilic triblocks

We first focused our attention on determining the conditions and volume fraction that would enable the fabrication of polymersomes using PEG-*b*-P(S-*stat*-CMA)-*b*-PEG. For soft block copolymers, the self-assembly can be conducted by directly hydrating the polymers with an aqueous solution.[26,33] However, we resorted to a solvent injection method for the self-assembly of PEG-*b*-P(S-*stat*-CMA)-*b*-PEG, since the glassiness of the P(S-*stat*-CMA) center block makes it extremely hydrophobic and therefore requires plasticization with an organic solvent.[34] Dioxane:THF 1:1 (v/v)[35] was used as the organic solvent mixture for it dissolved the PEG-*b*-P(S-*stat*-CMA)-*b*-PEG at all compositions. Upon dissolution, we slowly added deionized (DI) water via a syringe pump until we reached 50% by volume. Notably, the mixture turned cloudy around 20% by volume, suggesting that the self-assembly process had already begun at or before this composition. After the water addition was complete, an aliquot was then extracted and

subsequently quenched in vigorously stirring water, thus vitrifying the hydrophobic block and freezing the morphologies that formed.

2.2.1 Self-assembly behavior of PEG_{22} triblock copolymers

Using the aforementioned self-assembly procedure, PEG_{22}-*b*-P(S-*stat*-CMA)$_{56}$-*b*-PEG_{22} (Figure 1a), PEG_{22}-*b*-P(S-*stat*-CMA)$_{104}$-*b*-PEG_{22} (Figure 1b) and PEG_{22}-*b*-P(S-*stat*-CMA)$_{118}$-*b*-PEG_{22} (Figure 1c) formed polymersomes. Comparatively, PEG_{22}-*b*-P(S-*stat*-CMA)$_{136}$-*b*-PEG_{22} yielded a mixture of large compound micelles and vesicles (Figure 1d), suggesting that under these conditions, the value of *f* was approaching a threshold where vesicles were no longer the most stable morphology.

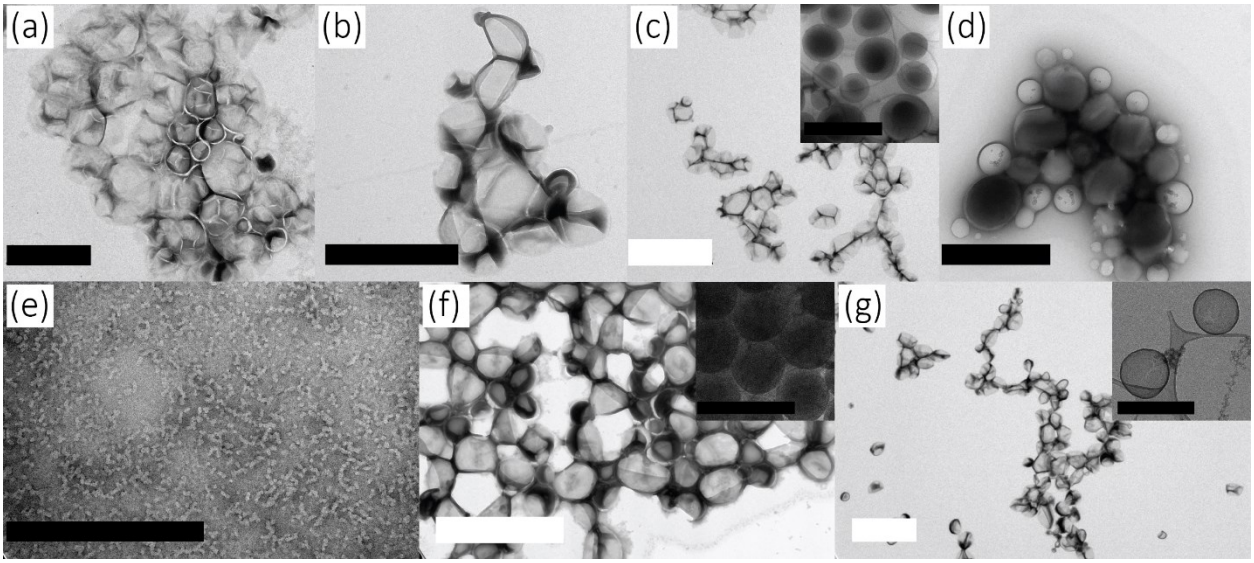

Figure 1. (a) Transmission electron micrographs showing the morphologies observed from the self-assembly of (a) PEG_{22}-*b*-P(S-*stat*-CMA)$_{56}$-*b*-PEG_{22} (*f*=19%) (b) PEG_{22}-*b*-P(S-*stat*-CMA)$_{104}$-*b*-PEG_{22} (*f*=12%) (c) PEG_{22}-*b*-P(S-*stat*-CMA)$_{118}$-*b*-PEG_{22} (*f*=11%) (cryo-TEM inset) (d) PEG_{22}-*b*-P(S-*stat*-CMA)$_{136}$-*b*-PEG_{22} (*f*=8%) (e) PEG_{45}-*b*-P(S-*stat*-CMA)$_{70}$-*b*-PEG_{45} (*f*=24%) (f) PEG_{45}-

b- P(S-*stat*-CMA)$_{170}$-*b*-PEG$_{45}$ (*f*=13%) (cryo-TEM inset) (g) PEG$_{45}$-*b*- P(S-*stat*-CMA)$_{206}$-*b*-PEG$_{45}$ (*f*=10%) (cryo-TEM inset). Scale bars: black, 1 μm; white 2 μm.

2.2.2. Self-assembly behavior of PEG$_{45}$ triblock copolymers

PEG$_{45}$-*b*-P(S-*stat*-CMA)$_{70}$-*b*-PEG$_{45}$ assembled into worm-like micelles (Figure 1e), indicating that *f* was too low to elicit the formation of vesicles. Gratifyingly, PEG$_{45}$-*b*-P(S-*stat*-CMA)$_{170}$-*b*-PEG$_{45}$ and PEG$_{45}$-*b*-P(S-*stat*-CMA)$_{206}$-*b*-PEG$_{45}$ formed vesicles upon self-assembly. These results showed that vesicles started forming at *f* close to 20% in the PEG$_{45}$ systems just like observations made using the shorter PEG$_{22}$ block. Membrane thickness is dependent on the polymer molecular weight.[25,36] As expected, dry and cryo-TEM results (Figure 1e-g) showed that the PEG$_{22}$-*b*-P(S-*stat*-CMA)$_{118}$-*b*-PEG$_{22}$ had a noticeably thinner membrane (~14 nm) than PEG$_{45}$-*b*-P(S-*stat*-CMA)$_{206}$-*b*-PEG$_{45}$ (~21 nm).

2.3. Effect of osmotic pressure changes induced by dialysis

The default shape for most vesicles is spherical for it constitutes the thermodynamically most stable morphology, which minimizes the surface-to-volume ratio. However, like their lipid-based counterparts, polymersomes can transform into different shapes in response to changes in their milieu. Giant unilamellar vesicles and even smaller unilamellar vesicles adopt oblate, prolate, spherocylindrical and other shapes as a response to factors such as mechanical force and osmotic pressure changes.[37] The area-difference elasticity (ADE) theory asserts that volume changes of the inner compartment of the vesicles drive their shape transformations. Osmotic pressure differences and concentration gradients between the vesicle interior and their surroundings will therefore cause an area mismatch which leads to shape transformation.[38]

After successfully identifying their fabrication conditions, we turned our attention to vesicles made from PEG_{45}-*b*-P(S-*stat*-CMA)$_{206}$-*b*-PEG_{45} and probed their ability to shape-transform. In comparison to other reported systems,[35,39] we hypothesized that the vesicle membrane thickness (~21 nm) would be enough to sustain the planned shape-transformation. To characterize the size changes, we used dynamic light scattering (DLS) at multiple angles to evaluate the angular dependence of the diffusion coefficient with the square of the scattering vector, q^2. We then compared this effective hydrodynamic diameter (D_h) to the D_h values obtained at each angle via CONTIN (Figure S9 and Table S5).[40,41] In view of this observation, the size data discussed here will be based on the effective D_h calculations from the angle-dependent DLS, while for visual purposes, the size distributions are displayed for a given indicated angle.

First, we investigated the response of the polymer vesicles to osmotic pressure differences induced by dialysis. When the polymersome suspension was dialyzed against DI water for two days, we observed a decrease in D_h from 450 nm to 410 nm, without a significant change in the polydispersity of the assemblies, suggesting that the initial polymersomes were still intact (Figure 2a-b). Note that for the sake of simplicity, we are using the average value of D_h for the rest of the discussion. Kim et al reported a similar decrease in size for the transformation of glassy polymersomes into stomatocytes for PS-*b*-PEG.[35] Upon removal of the organic solvent by dialysis, the glassy nature of the hydrophobic block at room temperature limits permeability of the water molecules, resulting in a decrease in hydrodynamic radius since the water could not replace the organic solvent. Surprisingly, we did not observe any transformation of polymersomes into stomatocytes or any other non-spherical morphologies (Figure 2a, inset AD). For successful long-lived transformation, the polymersome membrane needs to be flexible enough to allow for a shape change but rigid enough maintain the newly formed morphology and prevent water inflow.[39] These

results suggested that the vesicles satisfied the former but not the latter, hence the retention of the spherical morphologies.

2.4. Effect of UV crosslinking in the polymersome shape transformation.

Chemical modification of the polymersome membrane can also induce non-equilibrium conditions that foster the shape transformation of vesicles. For example, van Oers et al fabricated polymersomes with an azide-functionalized styrenic hydrophobic block, poly(ethylene glycol)-*b*-poly(styrene-*co*-4-vinylbenzyl azide).[42] When they added an external alkyne crosslinker to the vesicle suspension, the resulting alkyne-azide cycloaddition led to their transformation into tubular polymersomes. The crosslinker could not uniformly permeate the vesicle membrane, thereby creating a crosslinker gradient which led to an asymmetry of the bilayer membrane. We chose the coumarin-based derivative because of its biocompatibility and the rapid nature of the [2+2] cycloaddition dimerization reaction.[43] Furthermore, the facile crosslinking uses long wavelength UV light, does not require any external chemicals and the reaction can be performed at room temperature, thereby minimizing other changes in the vesicle environment which might inadvertently affect the vesicle properties under investigation.[44] When we irradiated PEG_{45}-*b*-P(S-*stat*-CMA)$_{206}$-*b*-PEG_{45}-based vesicles, the D_h of the vesicles slightly decreased from 450 nm to 443 nm presumably due to crosslinking-induced shrinking (Figures 2c-d). Note that despite the proximity of the two average values, each sequence saw a decrease in D_h, which further confirms that shrinking behavior upon crosslinking. The decrease of the characteristic absorbance peak at 319 nm further confirmed coumarin dimerization (Figure S10). Interestingly, the cryo-TEM images indicated membrane wrinkling (Figure 2c, inset AI). We also observed this wrinkling in the form of jagged edges on the membrane upon analysis by dry TEM (Figure S11b). We however

did not observe any tubular morphologies like van Oers et al.[42] We suspect that the UV irradiation ensured uniform crosslinking of the membrane, maintaining its equilibrium conditions.

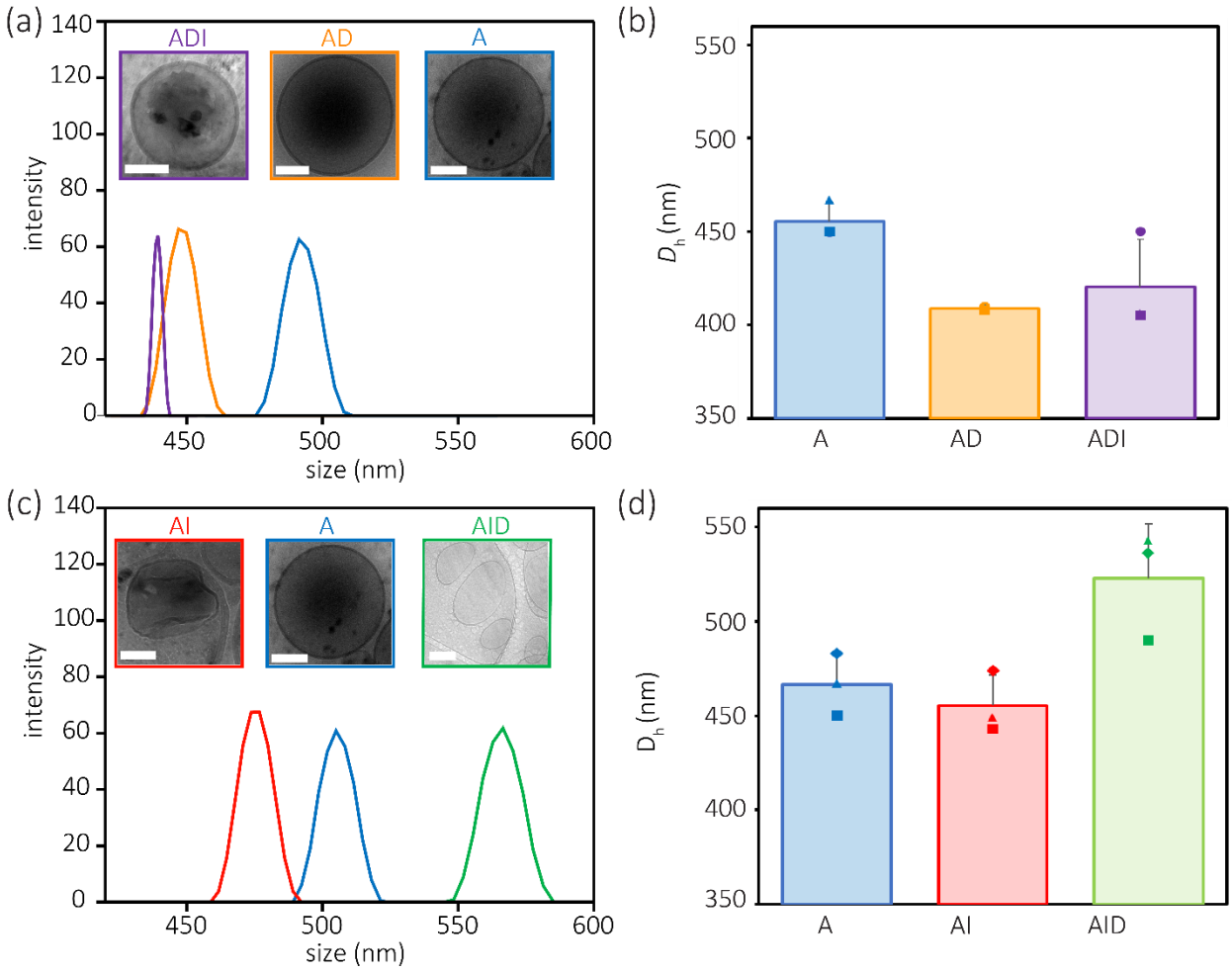

Figure 2. Analysis of the effect of UV-crosslinking, dialysis and combinations thereof on vesicle size and morphology for PEG_{45}-*b*-P(S-*stat*-CMA)$_{206}$-*b*-PEG_{45}. For each sample, the order of treatments, assembly (A), irradiation with UV (I) and dialysis (D), is represented by that of the corresponding letters. For the dialysis-first sequence, (a) DLS size distributions (at 120°) and corresponding cryo-TEM micrographs (insets) show the change in size of the polymersomes for each treatment while (b) the bar chart shows the variation in the average D_h extracted from the translational diffusion coefficient at multiple angles. For the crosslinking-first sequence, (c) DLS

size distributions (at 105°) and corresponding cryo-TEM micrographs (insets) show the change in size and morphology of the polymersomes for each treatment while (b) the bar chart shows the variation in the average D_h extracted from the translational diffusion coefficient at multiple angles. The DLS distribution graphs (a) and (c) were smoothed using the adjacent-average method and the dimension of the white scale bars for the TEM insets is 200 nm. For (b) and (d), each of the symbols (▲, ■, ◆, ●) corresponds to one replicate of the sequence.

2.4. Effect of combining UV crosslinking and dialysis

2.4.1. Effect of crosslinking dialyzed vesicles

When we irradiated the vesicles after dialysis, we did not observe any significant changes in the polymersome size (Figure 2a-b). The TEM images of the vesicles from this combination did not show any significant changes in the vesicle shape as the spherical morphology was retained (Figure 2a, inset ADI). This absence of morphological changes upon irradiation of the dialyzed vesicles is also observed in the dry TEM (Figure S12c).

2.4.2. Dialysis of crosslinked polymersomes

We then reversed the order of these processes by dialyzing the crosslinked polymersomes against DI water over two days. We expected that crosslinking would lower the permeability of the polymer vesicles and therefore even lead to a larger decrease in the vesicle size upon dialysis. However, after the initial slight decrease in size upon crosslinking, the hydrodynamic size of the vesicles increased upon dialysis to sizes larger than the initial assemblies (Figure 2c-d). Interestingly, the majority of these larger vesicles exhibited ellipsoidal morphologies via cryo-TEM (Figure 2c, inset AID). We also observed the same behavior when we carried out the same procedure on polymersomes from the self-assembly of PEG_{45}-*b*-P(S-*stat*-CMA)$_{170}$-*b*-PEG_{45}

(Figure S13). Since swelling could only be observed in the AID samples and not in ADI samples (Figures 2c-d), we posit that local shrinking upon crosslinking facilitated the formation of pores within the membrane of the polymersomes thereby eliciting their rapid swelling upon dialysis. We are currently investigating avenues to probe this phenomenon in greater depth.

To confirm that crosslinking played a role in this hypotonic response to dialysis, we synthesized a control triblock copolymer consisting a CMA-free center block flanked by two PEG blocks (PEG_{45}-*b*-PS_{403}-*b*-PEG_{45}) (Figure S14, SEC and ^{1}H NMR spectroscopy). After assembling into vesicles following the aforementioned procedure, we irradiated the polymersomes with UV-light and did not observe any significant size changes presumably on account of the absence of crosslinking (Figure 3). As anticipated and contrary to the coumarin-containing triblocks, the dialysis against DI water for two days led to a decrease in size. This result confirms that the crosslinking is directly responsible for the hypotonic behavior observed for PEG_{45}-*b*-P(S-*stat*-$CMA)_{206}$-*b*-PEG_{45}. Interestingly, upon dialysis, the polymersomes AID appear to undergo membrane fusion and to have a double-walled morphology (Figure 3e). This observation warrants further investigation that goes beyond the scope of the present study but was worth pointing out nonetheless. Interestingly, we also investigated the effect of crosslinking on the polymersomes in hypertonic conditions by dialyzing vesicles assembled from PEG_{45}-*b*-P(S-*stat*-$CMA)_{170}$-*b*-PEG_{45} against two different concentrations of a NaCl solution (25 mM and 50 mM). We again observed a decrease in the size of the uncrosslinked polymersomes after dialysis at both salt concentrations (Figures S16a and S17a), while the crosslinked vesicles showed a slight increase in size and aggregated in solution. The dry TEM images also suggested that the polymersomes still retained their shape under these hypertonic conditions (Figures S16b-d and S17b-d).

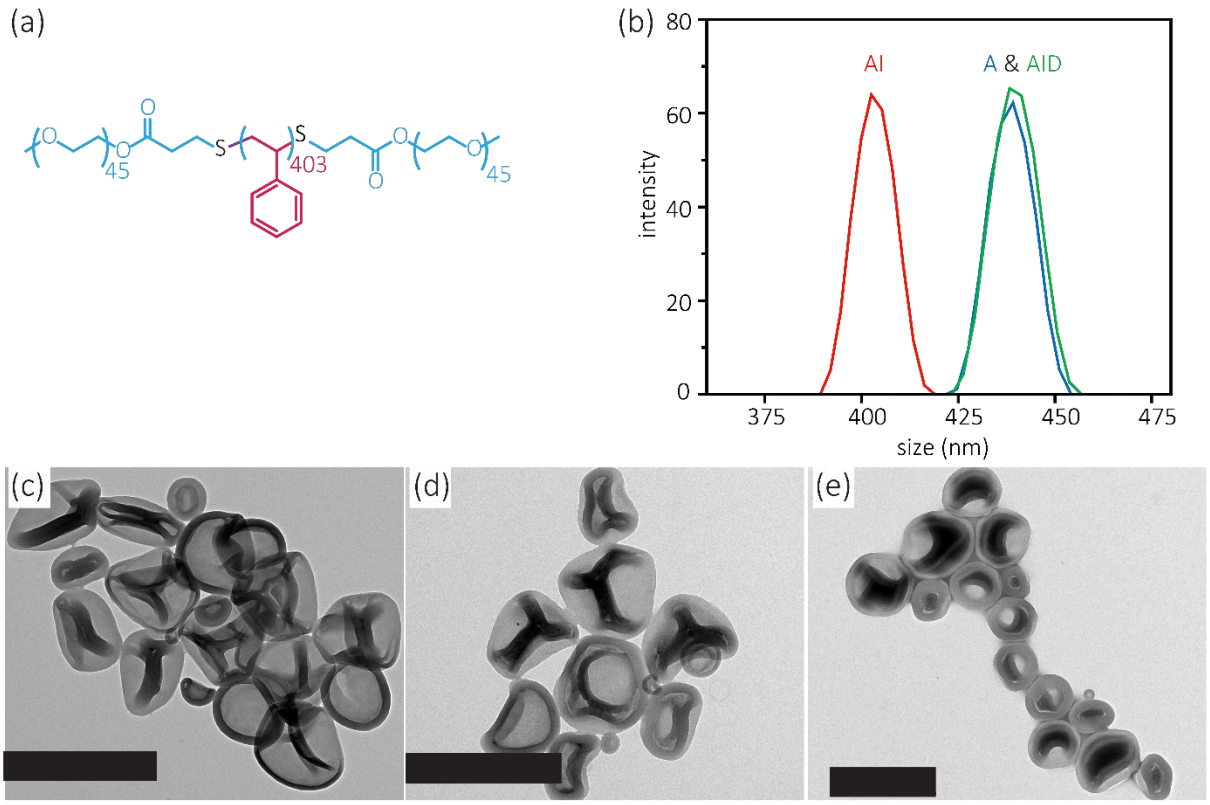

Figure 3. Representation of the control PEG_{45}-*b*-PS_{403}-*b*-PEG_{45} and assessment of its size and morphological changes upon assembly (A), crosslinking (AI) and dialysis (AID). (a) The scheme shows the chemical structure of PEG_{45}-*b*-PS_{403}-*b*-PEG_{45} (*vide supra* for an explanation of the depictional choices). (b) DLS size distribution (at 120°) showing the change in size of polymersomes after A, AI and AID. Corresponding TEM images showing the morphology of polymersomes from PEG_{45}-*b*-PS_{403}-*b*-PEG_{45} after (c) A, (d) AI and (e) AID.

2.5. Shape-transformation via PEG-induced rapid osmotic pressure changes

We then adapted a method recently demonstrated by Men et al to induce faster shape transformation using a low concentration of PEG as an additive.[39,45] PEG is a known fusogen with a dehydration effect on the membrane and a single ethylene oxide unit can bind up to three water molecules, creating an osmotic gradient.[38] In contrast to the osmotic pressure changes that rely on

dialysis, this method results in immediate shape change of polymersomes, with these transformations observed in less than a minute. Men et al observed that the PEG-induced osmotic gradient could be increased by either increasing the concentration or the molecular weight of the PEG additive.

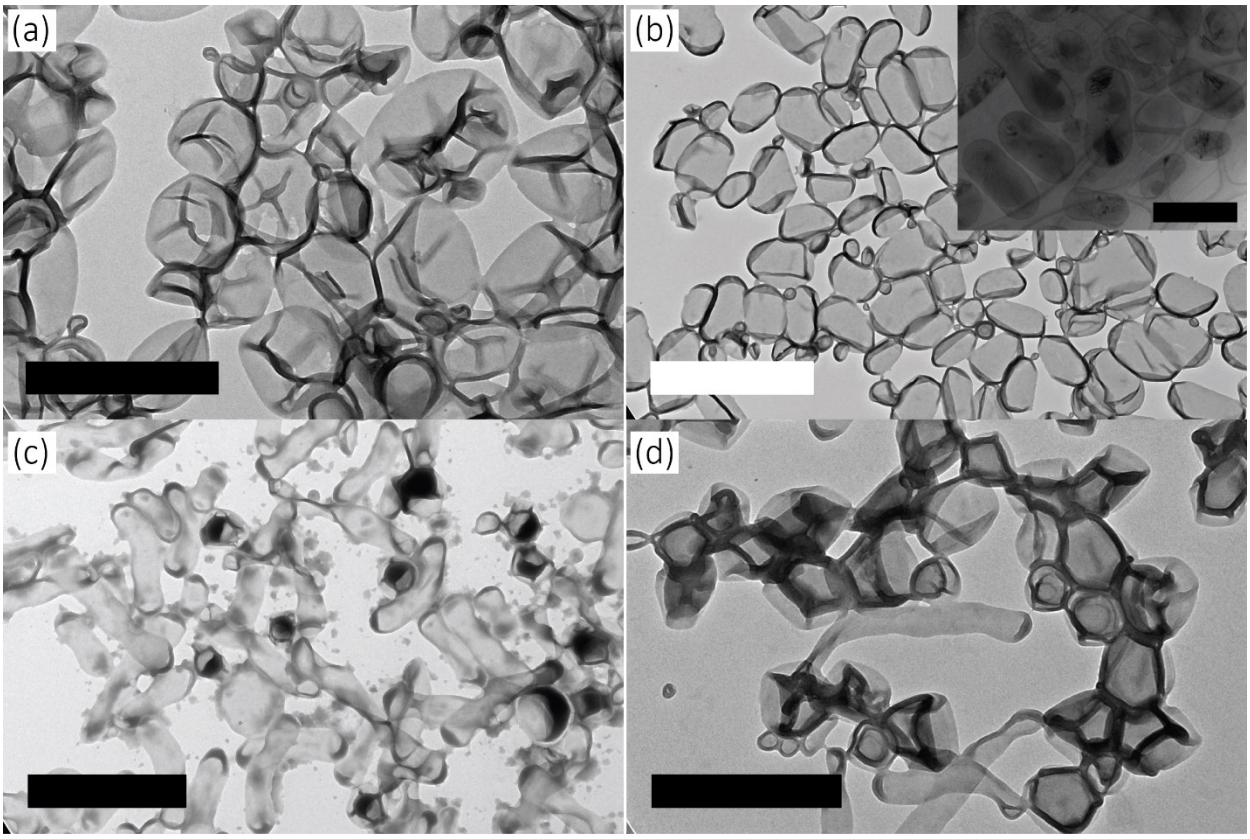

Figure 4. TEM images showing the morphologies observed (a) upon assembly (b) tubular polymersomes at 0.5 mg/mL PEG (cryo-TEM inset) (c) rod-like tubular polymersomes at 1 mg/mL PEG (d) stomatocyte-like morphology at 5 mg/mL PEG. Scale bars: black, 1 μm; white 2 μm.

We carried out the rapid osmotic change investigations using three different concentrations of a solution of 2 000 g/mol PEG, namely 0.5 mg/mL, 1 mg/mL and 5 mg/mL. In a typical procedure, we dissolved PEG_{45}-*b*-P(S-*stat*-CMA)$_{206}$-*b*-PEG_{45} in THF:dioxane 1:1 (v/v) and slowly added water at a rate of 1 mL/h until the aqueous composition reached 20% by volume (unlike the

50% by volume in the previously described procedure). We chose a high organic solvent composition to elicit shape change in view of the seemingly high flexibility of the polymersome membranes (cf. absence of transformation upon dialysis demonstrated in section 2.3). We subsequently transferred an aliquot of the suspension to a vial, added the PEG solution, centrifuged the mixture and quenched it in water. As a control, we performed a similar experiment in the absence of PEG additive and without centrifugation.

With increasing fusogen concentration, the vesicle morphology transformed from spheres, to ellipsoids, to tubes and eventually to a mixture of tubes and folded stomatocyte-like structures (Figure 4). Men et al. described a similar trajectory for PS_n-*b*-PEG_{45} diblock copolymers.[45] However, they could not observe any sustainable shape change for PS_{160}-*b*-PEG_{45} ($f = 10.7$) with a hydrophobic block of 16 700 g/mol. Compellingly, PEG_{45}-*b*-P(S-*stat*-CMA)$_{206}$-*b*-PEG_{45} triblocks could sustain the deformation and deviation from spherical morphology at $f = 10\%$, i.e. for a center block of 32 000 g/mol (< 33 400 g/mol = 2 x 16 700 g/mol). Although the hydrophobic blocks are different, this result points towards the anticipated enhanced sturdiness of the triblock copolymers compared to their diblock analogs and their consequent ability to promote shape transformation. It is interesting to observe that no permanent shape transformation occurred upon slow dialysis conditions while the rapid fusogen methods led to more stable non-spherical assemblies signifying the importance of kinetics in the shape transformation process.

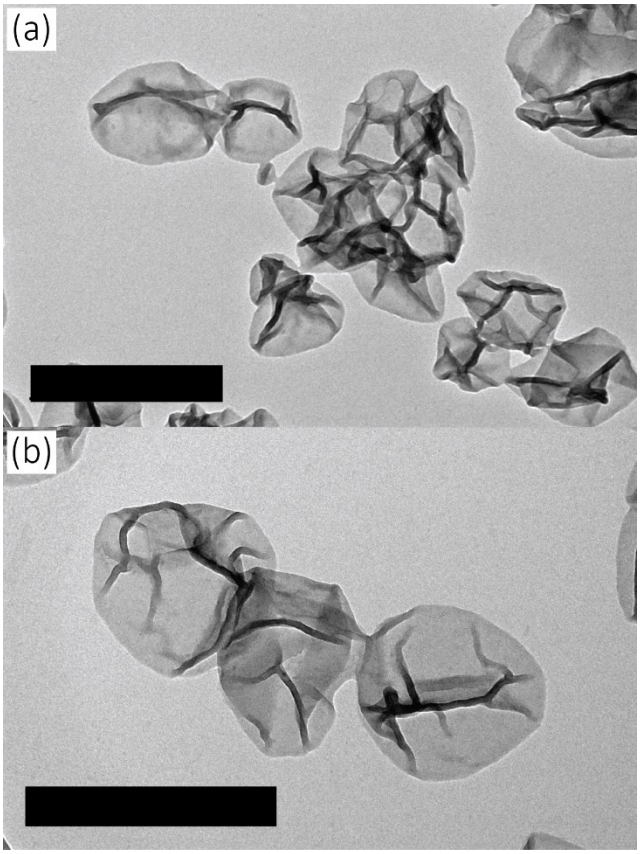

Figure 5. TEM images showing the effect of rapid osmotic pressure changes on crosslinked polymersomes. Morphologies observed various crosslinked polymersomes at PEG concentrations (a) 0 mg/mL and (b) 5 mg/mL. Scale bars: 1 μm.

After confirming that the triblock-based system could lead to successful shape-transformation of polymer vesicles, we were still curious about investigating the role of crosslinking in altering the polymersome membrane. To carry out this investigation, we first crosslinked the polymersomes before exposing them to osmotic pressure changes via PEG. Unlike the uncrosslinked polymersomes, no shape-transformation took place, suggesting that the crosslinking does affect the membrane makeup in such a way that affects its response to osmotic pressure changes. The polymersomes showed some wrinkling upon crosslinking, but there were no apparent morphological changes (Figure 5). The absence of shape transformation is even clearer

on the more concentrated sample with 5 mg/mL PEG concentration (Figure 5c). In the future, we also intend to investigate whether inducing coumarin dimerization after the shape transformation would also lead to further morphological changes.

3. Conclusion

In this work, we have shown that polymersomes from the self-assembly of glassy amphiphilic ABA triblock copolymers can be transformed into stable non-spherical morphologies. In addition to the membrane rigidity, the speed of the shape transformation also plays an important role in determining whether metastable morphologies can form. While slower osmotic pressure changes through dialysis only resulted in size decreases, the faster PEG-induced osmotic pressure changes led to morphological transformations of these polymersomes. We also demonstrated that chemically altering the membranes through crosslinking led to the vesicles demonstrating hypotonic shock, deviating from the typical behavior of the glassy polymers, suggesting that rearrangement of the membrane during crosslinking increases the permeability of the membranes. We believe that this phenomenon is very interesting to create triggered response of polymersomes in a variety of systems. Furthermore, we triggered this shape transformation of polymersomes with membranes whose diblock analogs are usually too short to sustain stable non-spherical shapes. This work demonstrates the complexities associated with membrane flexibility and dynamics in glassy polymersomes. Moreover, these results discussed highlight opportunities for utilizing facile and easily accessible chemical modifications which can play an important role in enhancing the use of these polymersomes as both cellular or organelle mimics and as delivery agents. In addition to designing a phase diagram of the morphologies that can be obtained from our polymersomes via rapid osmotic pressure changes, we also intend to do a comparative study of the diblock-based systems and triblock-based systems from our polymer system.

4. Experimental section

4.1. Materials

Styrene (Sigma Aldrich) was filtered through basic alumina to remove inhibitor before use. Tetrahydrofuran (THF), chloroform and *N,N*-dimethylformamide (DMF) were purchased from Fisher Scientific and were collected from a solvent purification system (PureSolv MD 5, INERT Technology). The monomer precursors 7-(2-hydroxyethoxy)-4-methylcoumarin (Alfa Aesar, 97%), ethylene carbonate (Acros, 99+%), triethylamine (Fisher Chemical, reagent grade), and sodium sulfate (Fisher Chemical)) were used as received. Methacryloyl chloride (Aldrich, 97%) was stored at -10 °C prior to use. Methoxy poly(ethylene glycol), (2 000 g/mol) (Sigma Aldrich), poly(ethylene glycol) methyl ether acrylate (2 000 g/mol and 1 000 g/mol PEG acrylate) (Sigma Aldrich) tributylphosphine (Sigma Aldrich) and *n*-hexylamine (Acros, 99%) were used as received. The RAFT agent precursors, sodium hydride (Acros), ethane thiol (Acros, 97+%), carbon disulfide (Sigma Aldrich), I2 (Acros), sodium thiosulfate (Fisher Chemical), 4,4′-azobis(4-cyanopentanoic acid) (V-501) (Alfa Aesar), ethylene glycol (Fisher Chemical), *N*,*N*′-dicyclohexylcarbodiimide (DCC) (Avocado Research Chemicals), and *N*,*N*-dimethyl-4-aminopyridine (DMAP) (Acros) were used as received. The solvents diethyl ether (Fisher Chemical), dichloromethane (DCM) (Fisher Chemical), methanol (Fisher Chemical, ACS grade) and *n*-pentane (Fisher Chemical) were used as received. The initiator 2,2′-azobis(2-methylpropionitrile) (AIBN) (Sigma Aldrich, 96%) was recrystallized in methanol prior to use. Methanol (Fisher Chemical) used in polymer precipitations was kept in the fridge at 4 °C. Type II Millipore deionized (DI) water was used throughout the process. The DI water used to quench samples was further passed through a 0.2 μm PTFE membrane filter before use. Regenerated

Cellulose Dialysis Tubing (Fisherbrand, MWCO 12-14kDa) was soaked in DI water for 1 hour and washed with at DI water (1 L) before use.

4.2. Methods

4.2.1. Nuclear magnetic resonance spectroscopy (NMR)

^{1}H NMR spectra were recorded on a Varian MERCURY 300 MHz and 600 MHz Bruker AVANCE III spectrometers. ^{13}C NMR spectra were recorded at 150 MHz on the Bruker AVANCE III spectrometer. All chemical peaks were referenced to TMS at 0 ppm for ^{1}H NMR and ^{13}C NMR spectra were recorded at 298 K.

4.2.2 Flash Chromatography

Column chromatography was done using a Biotage Isolera One flash purification system with a 200-400 nm variable detector, using pre-packed Snap Ultra 10 g or 25 g cartridges (Biotage).

4.2.3. Size-exclusion chromatography (SEC)

SEC was performed using a Wyatt GPC consisting of a Waters Alliance 2695 separations module and an interferometric refractometer (refractive index detector, Optilab TrEX, Wyatt Technology Inc.) (operating at 35 °C and 685 nm), an on-line multi-angle laser light scattering (MALLS) detector fitted with a gallium arsenide laser (power: 20 mW) operating at 658 nm (miniDAWN TREOS, Wyatt Technology Inc.), and two PLgel (Polymer Laboratories Inc.) mixed 3E columns (3 μm bead size, pore size range 50-103Å,). Freshly distilled THF was used as the mobile phase at a flow rate of 1.0 mL/min and sample volume of 100 μL was injected for each run. All the detector signals were recorded and analyzed using ASTRA 6 software (Wyatt Technology Inc).

The refractive index increments values were calculated from the refractive index detector response assuming 100% mass recovery for use with MALLS to determine the absolute molecular weights.

4.2.4. UV-vis spectrometry

All UV-vis absorbance spectra were measured on a Lambda 35 UV-vis Spectrophotometer (Perkin Elmer) equipped with a deuterium (UV light source) and halogen (Visible light source) lamp. Measurements were performed at a scan speed of 480 nm/min and a lamp change occurred at 326 nm. Samples were prepared by diluting 50 µL of the polymersome suspension with 2.95 mL of dry THF before transferring them to a 3 mL-quartz cuvette (Hellma 111-QS) with a 10 mm x 10 mm light path.

4.2.5. Dynamic light scattering (DLS)

DLS measurements were collected using incident light at 633 nm from a Research Electro Optics HeNe laser operating at 40 mW. The time-averaged scattering intensity (over two min) was measured from a Brookhaven Instruments BI-200SM goniometer with an avalanche photodiode detector and TurboCorr correlator.

4.2.6. UV-crosslinking

UV irradiation was conducted using a Hönle Bluepoint 4 UV light source (320-390 nm).

4.2.7. Transmission Electron Microscope (TEM)

Cryogenic-TEM (cryo-TEM) images were collected using a FEI G2 F30 Tecnai TEM instrument operated at 200 kV. Samples were prepared by placing a drop (5 µL) of the polymersome suspension on a carbon-coated TEM grid (Electron Microscopy Sciences). Using an automated Vitrobot (FEI) system at 100% humidity, the film was blotted for 5 s with a Whatman filter paper

and then vitrified in liquid ethane cooled by liquid nitrogen. The sample was then transferred onto a single-tilt cryo-specimen holder for imaging. The specimens were maintained below -175 °C during imaging. Membrane thicknesses for PEG_{22}-*b*-P(S-*stat*-CMA)$_{118}$-*b*-PEG_{22} and PEG_{45}-*b*-P(S-*stat*-CMA)$_{206}$-*b*-PEG_{45} were measured using ImageJ software and an average thickness of 10 different areas of the membrane was calculated.

Dry TEM was performed using a JEM-1400 TEM microscope at an acceleration of 60 kV. The samples were prepared by placing a drop (5 μL) of the polymersome suspension on a fresh carbon-coated TEM grid (Electron Microscopy Sciences). The specimen was allowed to dry in air for at least 30 minutes before imaging.

4.2.8. Data processing and presentation

All graphs were plotted using Origin Pro 2016 software (Origin Lab) and Microsoft Excel (Office 365, Microsoft), and figures were assembled using Adobe Illustrator software. Membrane thickness was obtained using ImageJ software (National Institutes of Health, Bethesda, MD) by calculating the average thickness from 10 measurements at different areas of the membrane.

4.3. Synthetic procedures

4.3.1. Synthesis of 7-(2-methacryloyloxyethoxy)-4-methylcoumarin (CMA)

The synthesis of 7-(2-hydroxyethoxy)-4-methylcoumarin was conducted following a previously reported procedure.[46] The product was collected as an off-white powder with a yield of 85% and used without further purification. ^{1}H NMR (300 MHz, DMSO-d_6, δ, ppm): 7.70–7.60 (m, 1H), 7.00–6.89 (m, 2H), 6.18 (d, 1H), 4.91 (t, 1H), 4.08 (t, 2H), 3.73 (dd, 2H), 2.38 (d, 3H).

The CMA was adapted from a previously reported procedure.[30] In a one-neck 250 mL Schlenk flask mounted with a stir bar and equipped with a PTFE stopcock, 7-(2-hydroxyethoxy)-4-methylcoumarin (8.00 g, 36.3 mmol, 1.0 equiv.) were dissolved in chloroform (100 mL) under a nitrogen atmosphere. Following the addition of triethylamine (10.13 mL, 72.65 mmol, 2.0 equiv.), the mixture was stirred at 0 °C for 15 minutes. Then, methacryloyl chloride (7.097 mL, 72.65 mmol, 2.0 equiv.) was added dropwise to the mixture at 0 °C, which was stirred for 16 hours under a nitrogen atmosphere. After 16 hours, the reaction mixture was treated with DCM and the organic layer was washed with brine (2 x 100 mL). The organic layer was then dried over $MgSO_4$ and the solvent was removed under reduced pressure via rotary evaporation. The crude product was further purified by recrystallization in ethanol to obtain white powdery crystals with a yield of 65%. ^{1}H NMR (300 MHz, $CDCl_3$, δ, ppm): 1.96 (s, 3H), 2.4 (s, 3H), 4.28 (t, 2H), 4.53 (t, 2H), 5.60 (s, 1H), 6.15 (s, 2H), 6.8–6.9 (m, 2H), 7.5 (d, 1H).

4.3.2. Synthesis of diCEP

CEP was synthesized based on a previously reported procedure.[47] In a 500-mL two-neck round-bottom flask, a suspension of (95%) NaH (2.11 g, 83.5 mmol, 1.0 equiv.) in anhydrous diethyl ether (150 mL) and was cooled to 0 °C in an ice/water bath. Ethane thiol (5.73 g, 92.3 mmol, 1.1 equiv.) was then added over 15 min accompanied by vigorous evolution of hydrogen gas. The reaction was stirred for an additional 15 min at 0 °C. Then, carbon disulfide (7.03 g, 92.3 mmol, 1.1 equiv.) was added dropwise over 5 min at 0 °C. The ice bath was then removed and the reaction was stirred for 60 min and allowed to warm back up to room temperature. Upon addition of pentane (100 mL), a yellow precipitate formed. The precipitate was then vacuum filtered with a Büchner funnel and dried *in vacuo* to yield sodium ethyl trithiocarbonate as a yellow powder. In a 500-mL two-neck round-bottom flask, a portion of the sodium ethyl trithiocarbonate (9.89 g,

61.7 mmol, 1.0 equiv.) was then suspended in diethyl ether (200 mL) at room temperature and solid I_2 (8.63 g, 34.0 mmol, 0.55 equiv.) was slowly added to the suspension. The reaction was stirred at room temperature for 60 min and a precipitate of NaI salts formed. The precipitate was then removed by vacuum filtration over a Büchner funnel and washed with diethyl ether (50 mL). The filtrate was then collected and transferred to a separatory funnel where it was washed with 5% sodium thiosulfate (2 x 150 mL), H_2O (1 x 150 mL), and brine (1 x 150 mL). The organic layer was then dried over magnesium sulfate and the solvent was removed under reduced pressure via rotary evaporation. A yellow powder was obtained and dried in a vacuum oven at room temperature to obtain bis(ethyl) trithiocarbonate as a yellow solid. In a 500 mL 3-necked round-bottom flask equipped with stir bar and condenser, bis-ethyltrithiocarbonate (5.00g, 18.2 mmol, 1.0 equiv.) and V-501 (7.66 g, 27.3 mmol, 1.5 equiv.) were dissolved in EtOAc (250 mL). The solution was purged with N_2 for 45 mins and then heated to reflux for 18 hours. The reaction was quenched via exposure by opening the reaction vessel to air and cooling to room temperature. A yellow powder was obtained under reduced pressure via rotary evaporation under vacuum, and then purified via flash column chromatography hexanes/EtOAc/Acetic acid (60/35/5, v/v, R_f = 0.4). The column fractions containing CEP were transferred into a separatory funnel and washing with 0.05 N HCl (2 x 150 mL), and brine (1 x 150 mL). The organic layer was dried over $MgSO_4$, and the solvent was removed under reduced pressure via rotary evaporation followed by drying in a in a vacuum oven overnight at room temperature to yield CEP as a yellow solid.

Yield: 7.10 g (74%); ^{1}H NMR (300 MHz, $CDCl_3$, δ, ppm): 3.38 (q, 2H), 2.70 (t, 2H), 2.55 (m, 2H), 1.85 (s, 3H), 1.40 (t, 3H).

CEP (2.09g, 7.96 mmol, 2.20 equiv.) was added to a 100-mL two-neck round-bottom flask equipped with a stir bar under nitrogen atmosphere. Ethylene glycol (0.22 g, 3.62 mmol, 1.00

equiv.) was then added to the flask followed by the addition of DCM (30 mL). The reaction vessel was then immersed in an ice and water bath. Separately, DCC (1.56 g, 7.60 mmol, 2.10 equiv.) and DMAP (0.09g, 0.76 mmol, 0.21 equiv.) were dissolved in DCM (5 mL) in a scintillation vial. The solution was added to the cooled flask dropwise over 5 min and the mixture was stirred overnight. The reaction mixture was filtered to remove dicyclohexylurea and the salts were washed with DCM until white (ca. 10 mL). The filtrate was collected into an evaporating flask and the solvent was removed under reduced pressure in a rotary evaporator. The crude product was isolated by flash column chromatography ethyl acetate/ hexanes (v/v, 2/3, R_f = 0.48). The eluent was removed under reduced pressure by rotary evaporation to yield yellow gel (43% yield). ^{1}H NMR (600 MHz, $CDCl_3$, δ, ppm): 4.32 (s, 4H), 3.38 (q, 4H), 2.70 (t, 4H), 2.55 (m, 4H), 1.85 (s, 6H), 1.40 (t, 6H). ^{13}C NMR (150 MHz, $CDCl_3$, δ, ppm): 216.7 (s), 171.2 (s), 118.9 (s), 62.6 (s), 46.4 (s), 33.8 (s), 31.4 (s), 29.7 (s), 24.9 (s), 12.8 (s).

4.3.3. Representative RAFT for the homopolymerization of styrene and copolymerizations of styrene and coumarin methacrylate

In general, desired ratio of monomers, chain-transfer agent, and initiator were dissolved in dry DMF and added to a 25-mL Schlenk tube equipped with a magnetic bar. For example, styrene (1.9 g, 18.26 mmol, 426 equiv.), CMA (1.3 g, 4.50 mmol, 105 equiv.), diCEP (0.025 g, 0.043 mmol, 1.0 equiv.), AIBN (1.4 mg, 9.0 μmol, 0.2 equiv.) were dissolved in 3 mL of dry DMF and added to the Schlenk tube, which was then sealed and purged with argon gas for 30 minutes. After purging, an aliquot (0.2 mL) was taken, and the polymerization was started by plunging the reaction mixture into a pre-heated oil bath at 75 °C under constant stirring. After 20 hours, the reaction was quenched by opening the reaction vessel to air and the tube was cooled in liquid nitrogen for approximately 1 min. An aliquot (0.2 mL) was taken, and the remaining reaction

mixture was precipitated in cold methanol (45 mL). The mixture was centrifuged in 50-mL polypropylene tubes, the supernatant was decanted and the yellow precipitate was redissolved in DCM (5 mL). The solution was then precipitated in cold methanol (45 mL) and the centrifugation procedure was repeated twice. *Note that for a few samples ^{1}H NMR spectroscopy indicated the presence of residual monomer, and additional precipitations in cold methanol were needed to completely remove the monomer.* All polymers were characterized by SEC and ^{1}H NMR spectroscopy.

4.3.4. One-pot aminolysis and thia-Michael coupling

The hydrophobic block P(S-*stat*-CMA) underwent one-pot aminolysis and thia-Michael addition reaction, with either 1 000 g/mol or 2 000 g/mol PEG acrylate to obtain the triblock, PEG-*b*-P(S-*stat*-CMA)-*b*-PEG. For example, to a 100-mL round-bottom flask equipped with a stir bar under nitrogen, P(S-*stat*-CMA) (0.444 g, 0.014 μmol, 1.0 equiv.) and PEG acrylate (2 000 g/mol) (0.278 g, 139 μmol, 10 equiv.) were added. Using a syringe, dry THF (3 mL) was added to the flask to dissolve the polymers completely. Then, tributylphosphine (34.27 μL, 139 μmol, 10 equiv.) was added at once with a luer-lock gas-tight syringe (500 μL) and the reaction was allowed to stir for 15 minutes. *n*-Hexylamine (18.25 μL, 139 μmol) was added at once with a luer-lock gas-tight syringe (100 μL). After 18 hours, the solution was precipitated in a cold mixture of methanol:diethyl ether 10:1 (v/v) (16 mL). The mixture was centrifuged in 20-mL scintillation vial, the supernatant was decanted and the off-white precipitate was redissolved in THF (2 mL). The solution was then precipitated in methanol:diethyl ether 10:1 (v/v) (16 mL) and the centrifugation procedure was repeated twice. After confirming the removal of unreacted PEG acrylate via NMR, the triblock polymer was dried in vacuum over for overnight. All polymers were characterized by SEC and ^{1}H NMR spectroscopy.

4.4. Self-assembly and shape-transformation procedures

4.4.1. Procedure for the self-assembly process

The self-assembly procedure followed a previously published method.[35] In a 20-mL reaction vial with a rubber septum, PEG_{45}-*b*-P(S-*stat*-CMA)$_{206}$-b-PEG_{45} triblock polymer (20 mg) was dissolved in THF:Dioxane 1:1 (v/v) (2 mL). Upon dissolution, DI water (2 mL) was added to the solution under constant stirring (700 rpm) at 1 mL/h via a syringe pump. An aliquot (75 µL) of the cloudy suspension was then taken and quenched by addition to DI water (2 mL) under constant stirring (700 rpm). This sample was used for DLS measurements and TEM imaging.

4.4.2. Slow osmotic pressure changes via dialysis

The cloudy polymersome suspension was transferred to a dialysis bag (MWCO 12-14 kDa) which was then left in DI water (1 L) for 48 hours without any agitation. The DI water was changed every 12 hours. After dialysis, the polymersome suspension (75 µL) was also quenched in DI water (2 mL) under constant stirring (700 rpm) and then analyzed by DLS and TEM imaging.

4.4.3. Vesicle crosslinking via UV irradiation

The polymersome suspension was transferred to a 1-dram vial equipped with a stir bar in air. The suspension was then irradiated for 120 seconds in a closed chamber before another aliquot (50 µL) was taken for UV-vis analysis. An aliquot (75 µL) of the irradiated polymersome suspension was also quenched in DI water (2 mL) under constant stirring (700 nm) and then analyzed by DLS and TEM imaging.

4.4.3. Rapid osmotic pressure changes via PEG fusogen

The process was conducted following a previously reported procedure.[45] In a 20-mL reaction vial with a rubber septum, PEG_{45}-*b*-P(S-*stat*-CMA)$_{206}$-*b*-PEG_{45} polymer (10 mg) was dissolved in THF:Dioxane 1:1 (v/v) (1 mL). DI water was then added at a rate of 1 mL/h until the aqueous composition reached 20% by volume. An aliquot (50 μL) of the polymersome suspension was quenched by addition DI water (2 mL) under constant stirring. A portion (200 μL) of the cloudy polymersome suspension was then transferred to a 2-dram vial before the PEG solution (15μL of 0.5 mg/mL, 1 mg/mL or 5 mg/mL in DI water) was added. The PEG/polymersome mixture was centrifuged for one minute before an aliquot (50 μL) was quenched in DI water (2 mL) under constant stirring and analyzed via TEM imaging.

Conflicts of Interest

There are no conflicts to declare.

Acknowledgements

The authors would like to acknowledge Ying Xiao at the Shared Instrumentation facility at Louisiana State University and Dr. Jibao He at the Coordinated Instrumentation Facility at Tulane University for help with TEM imaging. This work was supported by the National Science Foundation through the CAREER (1945092) and EPSCoR (1757220) grants. EG would like to acknowledge financial support from the Drapeau Foundation.

References

1. C. K. Wong, A. D. Martin, M. Floetenmeyer, R. G. Parton, M. H. Stenzel and P. Thordarson, *Chem. Sci.*, 2019, **10**, 2725-2731.
2. T. Einfalt, D. Witzigmann, C. Edlinger, S. Sieber, R. Goers, A. Najer, M. Spulber, O. Onaca-Fischer, J. Huwyler and C. G. Palivan, *Nat. Commun.*, 2018, **9**, 1127.
3. E. Rideau, R. Dimova, P. Schwille, F. R. Wurm and K. Landfester, *Chem. Soc. Rev.*, 2018, **47**, 8572-8610.

4. P. Tanner, S. Egli, V. Balasubramanian, O. Onaca, C. G. Palivan and W. Meier, *FEBS Lett.*, 2011, **585**, 1699-1706.
5. Q. Chen, H. Schönherr and G. J. Vancso, *Small*, 2009, **5**, 1436-1445.
6. N. Ben-Haim, P. Broz, S. Marsch, W. Meier and P. Hunziker, *Nano Lett.*, 2008, **8**, 1368-1373.
7. Z. Wang, M. C. M. van Oers, F. P. J. T. Rutjes and J. C. M. van Hest, *Angew. Chem. Int. Ed.*, 2012, **51**, 10746-10750.
8. H. Zhao, V. Ibrahimova, E. Garanger and S. Lecommandoux, *Angew. Chem. Int. Ed.*, 2020, **n/a**.
9. J. R. W. Peters Ruud, M. Marguet, S. Marais, W. Fraaije Marco, C. M. van Hest Jan and S. Lecommandoux, *Angew. Chem. Int. Ed.*, 2013, **53**, 146-150.
10. J. S. Lee and J. Feijen, *J. Controlled Release*, 2012, **161**, 473-483.
11. J. Leong, J. Y. Teo, V. K. Aakalu, Y. Y. Yang and H. Kong, *Adv. Healthcare Mater.*, 2018, **7**, e1701276-e1701276.
12. M.-H. Lai, S. Lee, C. E. Smith, K. Kim and H. Kong, *ACS Appl. Mater. Interfaces*, 2014, **6**, 10821-10829.
13. W. H. Roos, I. L. Ivanovska, A. Evilevitch and G. J. L. Wuite, *Cell. Mol. Life. Sci.*, 2007, **64**, 1484-1497.
14. G. K. Voeltz and W. A. Prinz, *Nat. Rev. Mol. Cell. Biol.*, 2007, **8**, 258-264.
15. Y. Geng, P. Dalhaimer, S. Cai, R. Tsai, M. Tewari, T. Minko and D. E. Discher, *Nat. Nanotechnol.*, 2007, **2**, 249-255.
16. N. Nishiyama, *Nat. Nanotechnol.*, 2007, **2**, 203-204.
17. J. D. Robertson, G. Yealland, M. Avila-Olias, L. Chierico, O. Bandmann, S. A. Renshaw and G. Battaglia, *ACS Nano*, 2014, **8**, 4650-4661.
18. E. P. Furlani and K. C. Ng.
19. P. Decuzzi, W. Pasqualini R Fau - Arap, M. Arap W Fau - Ferrari and M. Ferrari.
20. M. Caldorera-Moore, N. Guimard, L. Shi and K. Roy, *Expert Opin. Drug Delivery*, 2010, **7**, 479-495.
21. R. S. M. Rikken, H. Engelkamp, R. J. M. Nolte, J. C. Maan, J. C. M. van Hest, D. A. Wilson and P. C. M. Christianen, *Nat. Commun.*, 2016, **7**, 12606.
22. C. K. Wong, A. F. Mason, M. H. Stenzel and P. Thordarson, *Nat. Commun.*, 2017, **8**, 1240.
23. D. A. Wilson, R. J. Nolte and J. C. van Hest, *Nat. Commun.*, 2012, **4**, 268-274.
24. Y.-L. Yang, M.-Y. Chen, H.-K. Tsao and Y.-J. Sheng, *PCCP*, 2018, **20**, 6582-6590.
25. F. Itel, M. Chami, A. Najer, S. Lörcher, D. Wu, I. A. Dinu and W. Meier, *Macromolecules*, 2014, **47**, 7588-7596.
26. R. Salva, J.-F. Le Meins, O. Sandre, A. Brûlet, M. Schmutz, P. Guenoun and S. Lecommandoux, *ACS Nano*, 2013, **7**, 9298-9311.
27. X.-P. Qiu and F. M. Winnik, *Macromolecules*, 2007, **40**, 872-878.
28. M. H. Allen, S. T. Hemp, M. Zhang, M. Zhang, A. E. Smith, R. B. Moore and T. E. Long, *Polym. Chem.*, 2013, **4**, 2333-2341.
29. A. J. Convertine, D. S. W. Benoit, C. L. Duvall, A. S. Hoffman and P. S. Stayton, *J. Controlled Release*, 2009, **133**, 221-229.
30. S. Onbulak and J. Rzayev, *Polym. Chem.*, 2015, **6**, 764-771.
31. S. Perrier, *Macromolecules*, 2017, **50**, 7433-7447.
32. D. E. Discher and A. Eisenberg, *Science*, 2002, **297**, 967.

33. C. P. O'Neil, T. Suzuki, D. Demurtas, A. Finka and J. A. Hubbell, *Langmuir*, 2009, **25**, 9025-9029.
34. T. Chidanguro, E. Ghimire, C. H. Liu and Y. C. Simon, *Small*, 2018, **14**, 1802734.
35. K. T. Kim, J. Zhu, S. A. Meeuwissen, J. J. Cornelissen, D. J. Pochan, R. J. Nolte and J. C. van Hest, *J. Am. Chem. Soc.*, 2010, **132**, 12522-12524.
36. R. Chandrawati and F. Caruso, *Langmuir*, 2012, **28**, 13798-13807.
37. H. Hotani, *J. Mol. Biol.*, 1984, **178**, 113-120.
38. H. Alimohamadi and P. Rangamani, *Biomolecules*, 2018, **8**, 120.
39. Y. Men, W. Li, G.-J. Janssen, R. S. M. Rikken and D. A. Wilson, *Nano Lett.*, 2018, **18**, 2081-2085.
40. S. Yu, T. Azzam, I. Rouiller and A. Eisenberg, *J. Am. Chem. Soc.*, 2009, **131**, 10557-10566.
41. S. W. Provencher and P. Štêpánek, *Part. Part. Syst. Charact.*, 1996, **13**, 291-294.
42. M. C. M. van Oers, F. P. J. T. Rutjes and J. C. M. van Hest, *J. Am. Chem. Soc.*, 2013, **135**, 16308-16311.
43. P. Samanta, K. Kapat, S. Maiti, G. Biswas, S. Dhara and D. Dhara, *J. Colloid Interface Sci.*, 2019, **555**, 132-144.
44. C. P. Kabb, C. S. O'Bryan, C. C. Deng, T. E. Angelini and B. S. Sumerlin, *ACS Appl. Mater. Interfaces*, 2018, **10**, 16793-16801.
45. Y. Men, W. Li, Y. Tu, F. Peng, G.-J. A. Janssen, R. J. M. Nolte and D. A. Wilson, *ACS Nano*, 2019, **13**, 12767-12773.
46. Y. Liu, B. Fan, Q. Shi, D. Dong, S. Gong, B. Zhu, R. Fu, S. H. Thang and W. Cheng, *ACS Nano*, 2019, **13**, 6760-6769.
47. B. A. Abel, Ph.D. Dissertation The University of Southern Mississippi, 2016.